INORGANIC CHEMISTRY FRONTIERS

CCS 中国化学会 CHINESE CHEMICAL SOCIETY

ROYAL SOCIETY OF CHEMISTRY

Palladium Bis-Pincer Complexes with Controlled Rigidity and Inter-Metal Distance

Journal:	*Inorganic Chemistry Frontiers*
Manuscript ID	QI-RES-09-2020-001111.R1
Article Type:	Research Article
Date Submitted by the Author:	21-Sep-2020
Complete List of Authors:	Yu, Cheng-Han; Texas A&M University Zhu, Congzhi; The University of Texas at Austin, Ji, Xiaozhou; Texas A&M University, Chemistry Hu, Wei; Tsinghua University, Electronic Engineering Xie, Haomiao; Texas A&M University System, Chemistry Bhuvanesh, Nattamai; Texas A&M University, Fang, Lei; Texas A&M University, Chemistry; Texas A&M University, Materials Science and Engineering Ozerov, Oleg; Texas A&M University, Chemistry

ARTICLE

Palladium Bis-Pincer Complexes with Controlled Rigidity and Inter-Metal Distance

Received 00th January 20xx,
Accepted 00th January 20xx

DOI: 10.1039/x0xx00000x

Cheng-Han Yu†, Congzhi Zhu†, Xiaozhou Ji, Wei Hu, Haomiao Xie, Nattamai Bhuvanesh, Lei Fang* and Oleg V. Ozerov *

We report a series of redox-active bis(pincer) Pd(II) complexes in which the redox active units are based on either a diarylamido or a carbazolide framework. Compounds **1** and **2** contain two full diarylamido/bis(pincer) PNP units connected either via an Ar-O-Ar linker (**1**) or an Ar-Ar bond (**2**). Compound **3** is a fused bis(pincer) where the two PNP units share an aromatic ring. Compound **4** is built around an indolo[3,2-*b*]carbazole core in which two NNN pincers share an aromatic ring similarly to **3**. These metal complexes all display two reversible oxidation waves with the ΔE values increasing in the order of **1** < **2** < **4** < **3**. The same trend in increasing electronic coupling emerges from the analysis of the IV-CT bands in the NIR portion of the optical spectra. The analysis of these compounds was further advanced by data from EPR spectroscopy, X-ray diffractometry, and DFT calculations. It is concluded that the monooxidized cations $\mathbf{2}^{+}$-$\mathbf{4}^{+}$ belong to Class III on the Robin-Day classification of mixed-valence compounds. Compound **4** possesses enforced near-planarity that enables delocalization of the unpaired electron in $\mathbf{4}^{+}$ across a broader conjugated sysem compared to $\mathbf{3}^{+}$.

Introduction

Arylamine derivatives are one of the most widely used structural components in the designs of organic functional materials for applications, such as electrochromic devices,[1,2] solar cells,[3,4] and light-emitting diodes.[5,6] Due to their electron-rich nature, arylamine derivatives can be readily oxidized into radical cations, whose persistence is dependent on the chemical environment and essential for the performance of organic electronic devices.[7,8]

The electronic structures and properties of organic aminyl radical cations can be modulated by coordination with transition metals.[9] The inductive effect of the transition metal as a substituent, the geometric consequences of the incorporation of the organic fragment into the coordination sphere of the metal, and the π-interactions between the p-orbital on the nitrogen atom and a d_{π} orbital of the metal center may all play a role. As a result, incorporating transition metals drastically changes the optical and electronic properties of such an organic radical. Transition metal-decorated analogues serve as promising unconventional building blocks in the development of organic electronic materials because they may allow a range of properties not attainable with organic molecules alone.[10–14] In addition, amido donors have in particular attracted attention as redox-non-innocent auxiliaries in the design of oxidizable pincer (tridentate, meridional) ligands.[15–22] Redox-active ligands in transition metal complexes have typically been studied in the context of supplementing the reactivity of the metal center in catalysis and in novel chemical transformations.[23–26] In a broader sense, we were interested in using coordination chemistry as a lynchpin to bring about new structures possessing extended conjugation in ligands, exotic redox activities, and synthetic potential for further connectivity.[27–29]

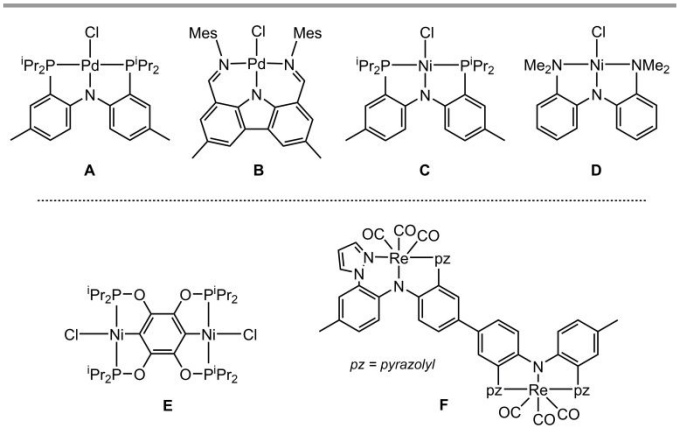

Figure 1. Top: selected examples of diarylamido-centered pincer complexes, whose reversible redox properties have been studied previously. Bottom: recent examples of Janus pincers in the literature.

Metal complexes of diarylamido-centered pincer ligands with two neutral side donors are a particularly well-behaved set of examples of ligand-based of redox-activity (Figure 1, top).[18–22,30] A broad synthetic variation of possible donor sets is possible,

[a] *Department of Chemistry, Texas A&M University, College Station, TX 77842, USA*
E-mail: fang@chem.tamu.edu and ozerov@chem.tamu.edu
† These authors contributed equally to this work.
Electronic Supplementary Information (ESI) available: details of experimental descriptions, characterization data, and graphical spectra . CCDC numbers: 1915569-1915571, 2003991, 2003992. See DOI: 10.1039/x0xx00000x

while maintaining reversibility of the oxidation and the apparent stability of the corresponding radical cation. The optical properties of these pincers in the complexes of group 10 metals (Ni, Pd, Pt) are strongly dependent on the identity of the transition metal, while the redox properties are affected by a change in the metal to only a modest degree because the oxidation primarily takes place at the ligand, with minimal electronic involvement of the metal.[19–22]

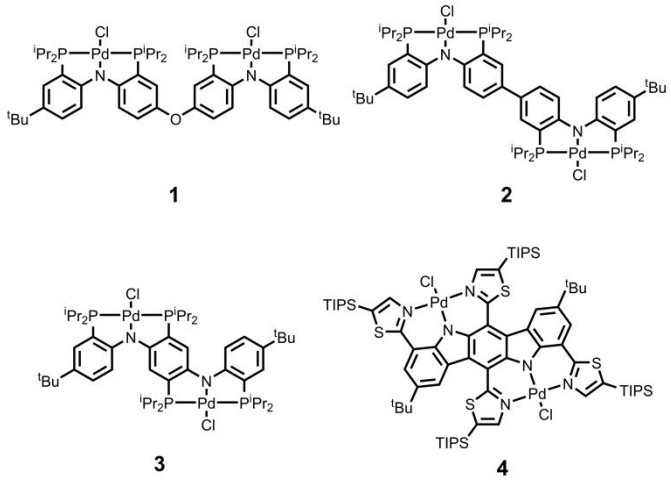

Figure 2. Bis(pincer) complexes synthesized and studied in this work.

With this background in mind, we became interested in exploring molecules that combine multiple diarylamido-centered pincer-complex moieties and in the electronic coupling possible between these different redox sites. A few years ago, we explored bimetallic bis(PNN)M complexes in which the two pincer cores were connected by a non-conjugating linker to a side arm donor.[31] More recently, we reported on the electronic communication in the bimetallic complexes where two (PNP)M cores are connected by ynediyl linkers,[32] i.e., via metal-ligand bonds. In this work, we set out to explore bimetallic complexes where the two redox sites are connected via organic ligand-to-ligand linkers that modulate the degree of separation between the redox sites. We targeted the four systems depicted in Figure 2. In this report, we present their syntheses and characterization of the degree of electronic coupling. Compounds **1** and **2** represent two (PNP)M cores connected via the *para*-positions of the individual PNP ligands, either by an oxygen atom (**1**) or by a direct aryl-aryl bond (**2**). Compound **3** brings the two core PNP units even closer by means of them sharing one of the aromatic rings. Compound **4** is related to **3** in that the two pincer cores share a central ring substituted by two *para*-nitrogens, but **4** is based on an indolo[3,2-*b*]carbazole, a high-performance *p*-type organic semiconducting molecule .[33] Consequently, **4** possesses a rigid and planar ligand, with a more extended conjugation in the backbone. We utilized thiazole side donors in **4** instead of phosphines for reasons of synthetic feasibility and also to create a less electron-rich system vs PNP. This results in two (NNN)M cores which can be related to the mononuclear complex **B**.

Compounds **1-4** are examples of the so-called Janus pincer systems, with two pincer cores on either end of the molecule "facing" in opposite directions. Janus pincer complexes have been studied previously, but the majority of reported systems are based on aryl-centered pincers[34–38] that are not intrinsically redox-active in a well-behaved, reversible fashion. The most recent example is the work by the Guan group on the Ni complexes of a Janus bis-POCOP ligand (**E**, Figure 1).[39] Gardinier et al. studied a Re complex of Janus bis-NNN pincer (**F**, Figure 1) that was built by connecting diarylamido cores similarly to **2**, although the fused analogues to **3** and **4** were not explored.[40] The bis-rhenium complex could be reversibly oxidized. However, the NNN ligand in Gardinier's compound adopted facial geometry about Re, thus not acting structurally as a pincer and disrupting potential conjugation with the lone pair at N, especially in contrast to a system such as **4**. Thus, while Gardinier's pioneering example was instructive, we were motivated to explore metal complexes with enhanced planarity and chose a square-planar Pd center with a low-spin d^8 configuration. The use of a divalent metal with monoanionic pincer cores additionally offers an "extra" Pd-Cl coordination site. Although it was not attempted in this work, the Pd-Cl moiety offers potential for facile further functionalization, something that is not easily possible with a $Re(CO)_3$ terminus.

Results and discussion

Preparation of bis-pincer Pd complexes

The syntheses of the bis(PNP) pincer pro-ligands and their Pd complexes were carried out as depicted in Scheme 1 and followed the general protocols we have previously established for the synthesis of mono-nuclear PNP pro-ligands.[22,41,42] First, Buchwald-Hartwig coupling[43–45] was utilized to couple dibromoarenes **5**-**7** with two equiv. of *tert*-butylaniline to give the bis(diarylamines) **8**-**10** in good yields. Bromination of **8**-**10** with *N*-bromosuccinimide (NBS) in CH_2Cl_2 proceeded selectively to give good yields of the desired quadruply *ortho*-brominated compounds **11**-**13** under mild conditions. Except for the more electron-rich central benzene in **10**, each aromatic unit was brominated only once under these conditions.[17,39,40] N-methylation of **11**-**13** was accomplished through deprotonation with NaH followed by treatment with methyl iodide, affording **14**-**16** in nearly quantitative yields.

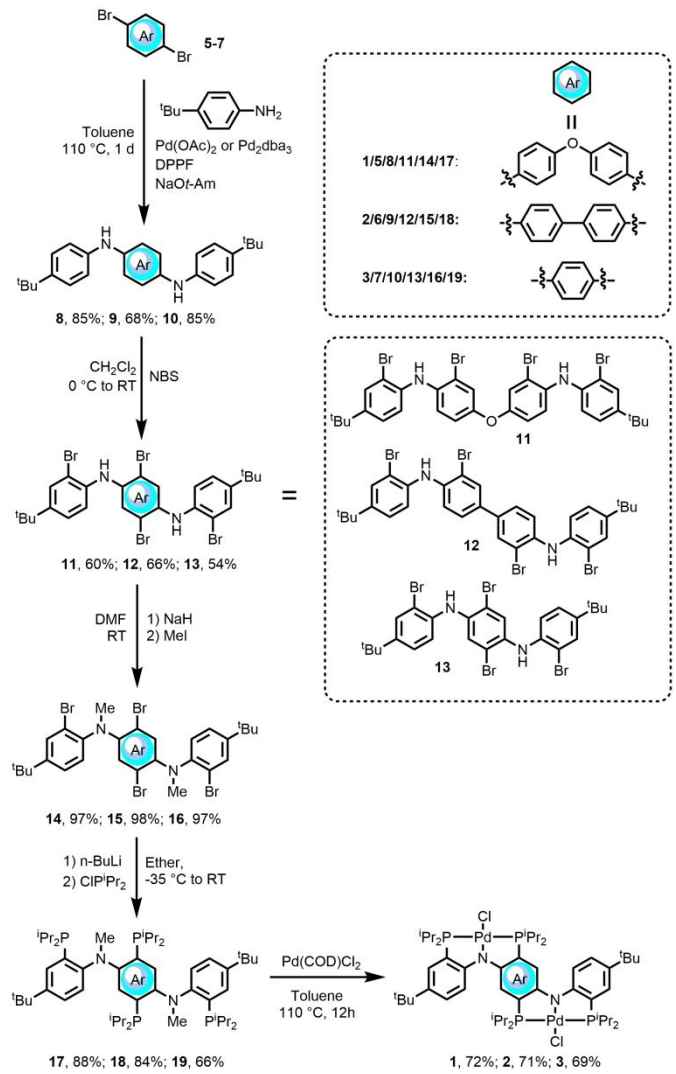

Scheme 1. Synthesis of bis(PNP) pro-ligands and their Pd complexes **1**-**3**.

Lithiation of **14**-**16** with ^{n}BuLi in diethyl ether followed by the addition of chlorodiisopropylphosphine led to the formation of **17**-**19**. Recrystallization from CH_2Cl_2/MeCN at -35 ºC afforded **17**-**19** in good isolated yields. We elected to pursue the syntheses of the N-methylated proto-pincers such as **17**-**19** as opposed to using **11**-**13** directly in the lithiation step for two reasons. Firstly, past work showed that the lithiation and the following phosphination of the mononuclear N-methylated brominated diarylamines proceeded cleanly and in many cases close to quantitatively, whereas the analogous lithiation/phosphination of the N-H versions typically did not.[22,41,42] The high selectivity towards the production of **17**-**19** was especially important because of the presence of the two pincer sites and because of the high lipohilicity and solubility of the products in organic solvents rendering any potential separation a challenge. Secondly, it was expected that the cleavage of methyl groups would proceed cleanly with Pd(II) reagents, as observed for the mononuclear PNP pro-ligands with –P^{i}Pr$_2$ groups.[22,41] Indeed, this expectation was justified and thermolysis of **17**-**19** with (COD)PdCl$_2$ afforded isolated yields of the desired bis-Pd complexes **1**-**3** of around 70% after workup.

The pro-ligands **17**-**19** and the dipalladium complexes **1**-**3** each possess two inequivalent phosphine sites, which can be thought of as the "outer" and the "inner" phosphines. This was reflected in the ^{31}P nuclear magnetic resonance (NMR) spectra of these compounds, which displayed pairs of closely spaced, but inequivalent ^{31}P resonances in the ranges of chemical shifts that were similar to the known mono-PNP analogues. The coupling between the two ^{31}P sites was 10 Hz in **17**-**19**, but significantly increased to above 410 Hz in **1**-**3**. Large $^{2}J_{P\text{-}P}$ values are typical for two *trans*-disposed phosphines in a late transition metal coordination sphere. (Table 1).

Table 1. Selected ^{31}P NMR data for **1**-**3** in C_6D_6.

	Pro-Ligand (δ ppm)	$J_{P\text{-}P}$ (Hz)	Pd Complex (δ ppm)	$J_{P\text{-}P}$ (Hz)
1	-5.70, -5.90	10	49.45, 47.45	418
2	-5.74, -6.02	10	48.86, 48.83	N/A
3	-4.34, -6.54	10	49.49, 44.66	414

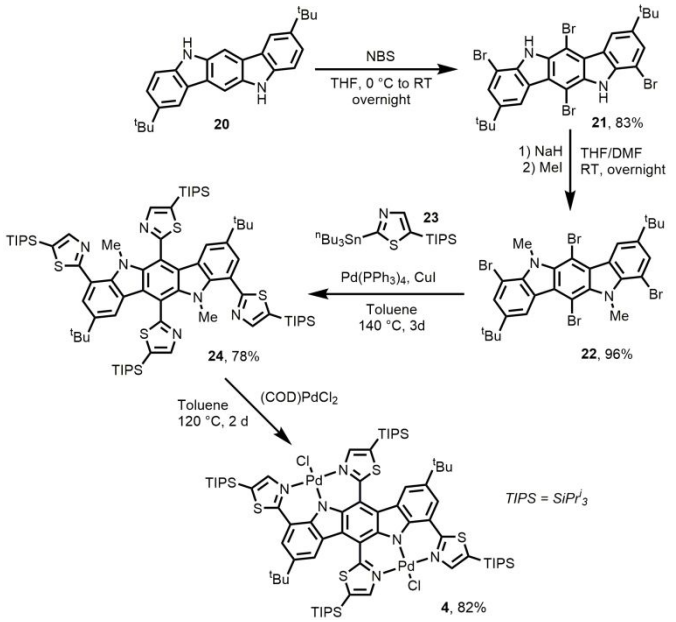

Scheme 2. Synthesis of Pd complex **4**.

Compound **4** was synthesized through a logically similar sequence (Scheme 2). The indolo[3,2-*b*]carbazole precursor **20** with *tert*-butyl groups was prepared according to a reported procedure.[27] Bromination of **20** with NBS proceeded selectively for all the positions *ortho* to the amine moieties, resulting in **21** in an excellent yield. N-methylation of **21** progressed smoothly to give **22**. Stille coupling[46,47] with the thiazole unit **23** proceeded well at 130 °C, and gave **24** in a high yield. Triisopropylsilyl (TIPS) groups were pre-installed on **20'** to endow the rigid and framework of **4** with high solubility. Gratifyingly, thermolysis of **24** with (COD)PdCl$_2$ did result in effective cleavage of the methyl groups,[30] and installation of two Pd(II) centers into the pincer clefts. The bimetallic complex

4 was air-stable under ambient conditions, and was purified by normal-phase silica gel chromatography.

Electrochemical analysis

Cyclic voltammetry (CV) studies of **1-4** were performed in CH_2Cl_2. The resulting CV plots are shown in Figure 3 and the corresponding electrochemical parameters are summarized in Table 2. All of the compounds **1-4** showed two quasireversible oxidation waves. The oxidation of **1-3** can be compared with the oxidation of the analogous mononuclear (PNP)PdCl complex **A**, which gives rise to a single quasireversible wave at -0.08 V vs the Fc/Fc^+ couple. As can be seen from Table 2, the increasing proximity of the two redox sites in the **1**-**3** series leads to the ever more negative potential for the first oxidation and the greater potential difference (ΔE) between the first and the second oxidation potential. This is especially pronounced for compound **3**, which possesses a central *p*-diaminobenzene unit. Compound **4** is more difficult to oxidize relative to **1-3**, because of the presence of the electron-deficient (relative to phosphines) thiazole units and because a carbazole framework is generally harder to oxidize than a diarylamido framework. Compound **4** can be compared with the (NNN)PdCl complex **B**, with its $E_{1/2}$ value of 0.69 V.[30] As was the case for **1**-**3** vs **A**, the first oxidation in **4** is considerably easier than in **B**.

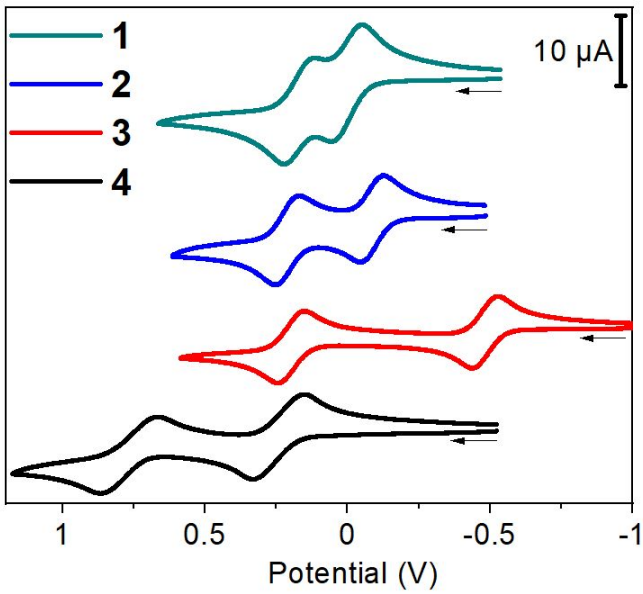

Figure 3. Cyclic voltammograms of **1**-**4** (ca. 0.001 M in CH_2Cl_2) with $[^nBu_4N]PF_6$ electrolyte (0.1 M), scan rate 100 mV/s, potentials referenced to Fc^+/Fc at 0 V.

Table 2 Summary of oxidation potentials.

	$E^1_{1/2}$ (V)	$E^2_{1/2}$ (V)	ΔE (V)	Kc
1	0.00	0.17	0.17	7.5×10^2
2	-0.13	0.21	0.34	5.6×10^5
3	-0.48	0.20	0.68	3.1×10^{11}
4	0.25	0.77	0.52	6.2×10^8

The ΔE values can be related to the comproportionation constant K_c.[48–50] These values are consistent with compounds **2, 3** and **4** belonging to the Robin-Day class III,[51,52] whereas the value for compound **1** falls into the range for class II. Caution must be exercised when evaluating electronic communication based only on the ΔE values, as was amply discussed by Winter.[48] The smaller ΔE value for **4** compared against 3 was surprising at first.[53] One might have expected **4** to display a greater stabilization effect toward $\mathbf{4}^+$ because **4** contains a π-system that is more coplanar and extended. However, it is possible that the more extended conjugation in **4** results in significant electron delocalization over the organic conjugated ligand, whereas in **3**, the redox events are more "concentrated" in the central *p*-diaminobenzene unit. This view is supported by the results of the DFT calculations (*vide infra*).

Solid-state structural characterization

Single-crystal diffraction was used to establish solid-state structures of compounds **1** and **3**, as well the oxidized derivatives $\mathbf{[2][CB_{11}H_{12}]_2}$, $\mathbf{[3]CB_{11}H_{12}}$, and $\mathbf{[3][SbCl_6]_2}$. Single crystals were obtained from solutions of **2** or **3** treated with an appropriate oxidant ($[Cp_2Fe]CB_{11}H_{12}$ or $[(p\text{-}BrC_6H_4)_3N]SbCl_6$, details in the ESI), although the oxidized compounds were not isolated on the preparative scale. The structures of **1** (see ESI, Figure S1) and **3** (Figure 4) confirmed the presence of two square-planar (PNP)PdCl moieties in these molecules. The metrics associated with the coordination environment of Pd in **1** and **3** closely mimicked those in the previously reported mononuclear (PNP)PdCl structure **A**.[54]

Interestingly, the overall shape of the bis(pincer) unit was very similar in the structure of **3** and in its oxidized derivatives $\mathbf{[3]CB_{11}H_{12}}$ and $\mathbf{[3][SbCl_6]_2}$ (see Figures S2 and S3). The geometric differences among these structures lie mainly in the changes in the distances associated with the central *p*-diaminobenzene unit (Table 3). The X-ray diffraction (XRD) data do not permit a finer analysis of the changes upon one-electron vs two-electron oxidation because of the relatively high esd values resulting from the solution of the structure of $\mathbf{[3]CB_{11}H_{11}}$. Nonetheless, oxidation clearly leads to the adoption of a more quinoidal structure with substantial C-C bond length alternation within the central ring and the shortening of the N-C bond to the central ring. In contrast, the aromaticity of the outer rings, the Pd-P and the Pd-N bond lengths are not significantly affected. On the other hand, the C-N distance to the outer ring elongates upon oxidation. These metric data support the notion of the dominance of the conjugation with the inner ring upon oxidation of **3**, illustrated in Figure 5 with the dominant quinoidal resonance structure for the doubly oxidized form of **3**.

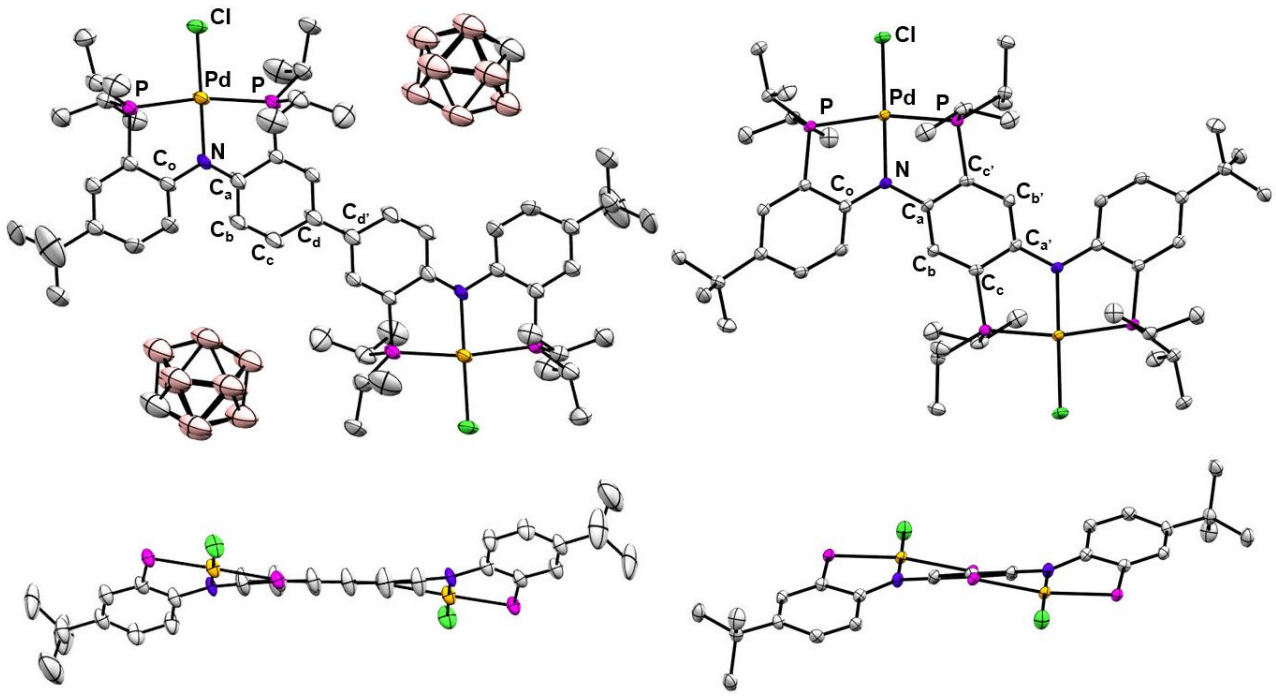

Figure 4. ORTEP drawings depicting the structure of **[2][CB$_{11}$H$_{12}$]$_2$** and **3**. Displacement ellipsoids are shown at the 50% probability level and all hydrogen atoms have been removed for clarity.

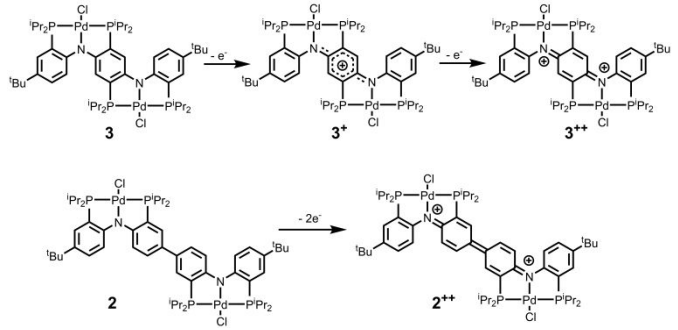

Figure 5. Dominant resonance forms upon oxidation of **2** and **3**.

Table 3. Selected distances (Å) in **3, [3]CB$_{11}$H$_{12}$, [3][SbCl$_6$]$_2$** and **[2][CB$_{11}$H$_{12}$]** (see Figure 4 for the numbering).

	3	**[3$^+$]**	**[3^{++}]**	**[2^{++}]^a**
Pd–N	2.0187(15)	2.024(9)	2.015(2)	2.027(5)
N–Ca	1.403(2)	1.350(17)	1.341(3)	1.339(7)
N–Co	1.383(2)	1.445(14)	1.419(3)	1.424(8)
Ca–Cb	1.403(3)	1.434(16)	1.441(4)	1.420(10)
Ca–Cf	1.408(3)	1.443(16)	1.444(4)	1.443(9)
Cb–Cc	1.397(3)	1.352(16)	1.360(4)	1.348(9)
Cc–Cd				1.44(1)
Cd–Cd'				1.430(9)

Similar arguments can be applied to the structure of **[2][CB$_{11}$H$_{12}$]$_2$** (Figure 4). The most striking features of the structure are the coplanarity of the two central aromatic rings and the distinct bond length alternation within the doubly oxidized central diaminobiphenyl unit. Figure 5 depicts the dominant quinoidal resonance structure for the **2^{++}** dication that dictates the coplanarity of the central rings.

Electron paramagnetic resonance (EPR) studies

Samples for the collection of EPR spectra (Figure 6) were prepared via addition of 0.9 equiv of [(*p*-BrC$_6$H$_4$)$_3$N]SbCl$_6$ to the CH_2Cl_2 solutions of the neutral compounds **1**-**4**, thus generating the monooxidized derivatives in situ. The recorded *g* values are close to the value for the free electron (*g* = 2.00232), consistent with the primarily ligand-based nature of the unpaired electron. Meanwhile, the *g* value decreasing (and approaches the free electron value) in the order **1** > **2** ≈ **3** > **4** was observed.

EPR spectra were simulated using EasySpin[55] as the red dashed lines in Figure 6, and the simulated coupling parameters are summarized in Table 4. For **1$^+$**, the best fit involved coupling to one *I* = 1 nuclei (^{14}N), and as well as coupling to two kinds of *I* = ½ nuclei (^{1}H or ^{31}P, four each). Similarly to the study of the mononuclear analogue **C$^+$** in 2008, we interpret these coupling constants as arising from coupling to ^{31}P or ^{1}H *ortho* to the nitrogen. For **2$^+$** and **3$^+$**, the best fit required considering two *I* = 1 nuclei (^{14}N) with additional coupling to another set of four *I* = ½ nuclei. The resolution of the spectra does not permit further effective modeling to analyze hyperfine coupling in **2$^+$** and **3$^+$**. The difference between a_N and the other coupling constants is largest in **3$^+$**. It could be the result of greater localization of the unpaired electron on the nitrogen sites.

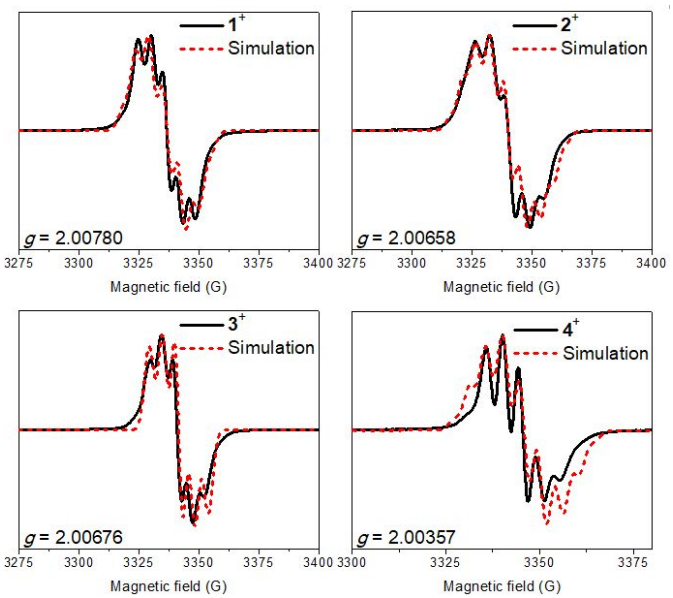

Figure 6. X-band EPR spectra (in black) of monocations [**1-4**] (ca. 0.01 M in CH_2Cl_2) generated in situ by treating **1-4** with 0.9 equiv. of $[(4\text{-}BrC_6H_4)_3N][SbCl_6]$. Instrumental parameters: T = 292 K; Freq = 9.38 GHz; Power = 0.6 mW, modulation 1 G. Simulations are shown in red (EasySpin).

Table 4 Summary of simulated coupling constants (a) (in G).

	a_N[a]	$a_{(P,H)}$[b]	$a_{(P,H)}$[b]	$a_{(P,H)}$[b]	$a_{(P,H)}$[b]	a_H[c]	a_H[c]
C$^+$	9.7	7.6	7.6	5.0	5.0	3.3	3.3
1$^+$	18.4	15.4	13.4	13.2	12.6		
2$^+$	18.6[d]	14.0	13.0	12.0	12.0		
3$^+$	14.5[d]	4.4	4.2	4.2	3.9		
4$^+$	27.8[d]					20.4[d]	20.2[d]

[a] Coupling constant to a I = 1 ^{14}N nucleus. [b] Coupling constant to an I = ½ nucleus (either ^{31}P or ^{1}H *ortho* to N_{amido}). [c] Coupling constant to an I = ½ nucleus assumed to be ^{1}H meta to N_{amido}. [d] Coupling to two nuclei

Lastly, the spectrum of **4**$^+$ was fitted by considering coupling to two N nuclei and two pairs of H nuclei *meta*- to the nitrogens. Notably, the coupling constants observed in **4** are larger than in **1-3**. It could be a consequence of a structure that is more rigid, with enforced coplanarity and enhanced π-orbital overlap, leading to the more effective delocalization of the unpaired electron.

Theoretical studies

Density functional theory (DFT) calculations (Gaussian 09 at the M06/LANL2DZp level)[56,57] were used to optimize the geometries of **1-4** and **1**$^+$-**4**$^+$ to analyze their electronic structure. In the DFT study of **4**, the $-Si^iPr_3$ substituents on the thiazole rings were replaced with -$SiMe_3$, and the *tert*-butyl groups on the indolo[3,2-*b*]carbazole were replaced with methyl groups for simplicity. The calculated geometries were generally in agreement with the results of the XRD structural determinations (*vide supra*). Figure 7 illustrates the comparison between the frontier orbitals in **3** and **4** and their mono-oxidized derivatives (the highest occupied molecular orbital (HOMO) and lowest unoccupied molecular orbital (LUMO) depictions for **1** and **2** can be found in the ESI, Figures S55 & S56). As expected, the HOMOs of both molecules and the corresponding singly occupied molecular orbitals (SOMO) for the monocations are primarily ligand-based, with marginal contribution from a d_π orbital at Pd. This is consistent with the past investigations of the mononuclear diarylamido-based pincer complexes.[19,22,58] In both **3** and **4**, the HOMO and SOMO is most prominent in the central diaminobenzene ring. However, in the case **4**, there appears to be a greater degree of delocalization across the broader ligand π-system. The greater delocalization in **4** dovetails the observation of lesser ΔE values (vs **3**) in the electrochemical studies and possibly also the higher coupling constants observed in the EPR spectrum of **4**$^+$ (vide supra).

On the other hand, the LUMOs in compounds **3** and **4** were calculated to be of a different nature. In **3** (as well as **1** and **2**), the LUMO can be thought of as the antibonding orbital corresponding to the σ-bonding in the plane of the Pd coordination sphere with the central contribution from the d_{z2} orbital of Pd.[58] However, in **4**, the LUMO corresponds to a π* orbital of the organic ligand system. This is likely owing to the conjugation with the electron-deficient thiazole, leading to the lower orbital energies of the π-system and . Only the central pair of the thiazole rings contributes to the LUMO.

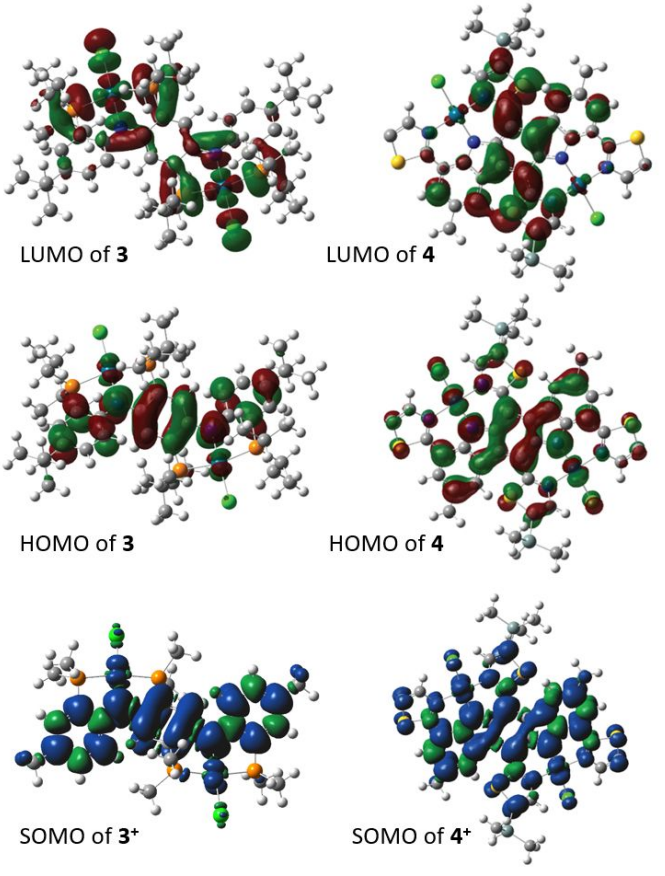

Figure 7. Depictions of the calculated LUMO, HOMO and SOMO for **3**/**3**$^+$ (left) and **4**/**4**$^+$ (right) (isovalue = 0.02). The silyl groups on the outer thiazole rings of **4**/**4**$^+$ have been removed from the graphic for clarity.

UV-Vis/NIR spectroscopic analysis

The UV-Vis/NIR[59] spectra of **1-4** and of their mono-oxidized derivatives **1**$^+$-**4**$^+$ were collected in CH_2Cl_2 (Figure 8). In the spectra of the neutral compounds **1**-**3**, the feature at ca. 500 nm appears at a wavelength similar to that observed in **A**. This is in

concert with the similar colors of the compounds: like **A**, compounds **1** and **2** are red, while compound **3** is purple. On the other hand, compound **4** is green and consequently shows a maximum at a higher wavelength. These observations are consistent with the different nature of the LUMO for **4** vs **1**-**3**, as revealed by the DFT studies. The HOMO-LUMO transition in **1**-**3** can be viewed as LMCT, while in **4** it is a π-π* transition for the ligand system, corresponding to lower energy. Notably the metal-free pro-ligands **17**-**19** are colorless and **24** is yellow. The apparent red shift of absorptions upon the introduction of the Pd center is related to a few factors. Pd is less electronegative than CH_3 and may be a modest π-donor towards the nitrogen which serves to raise the overall energy of the HOMO. For **1**-**3**, the introduction of the Pd center introduces a new, lower-energy, metal-based LUMO. In **4**, the lowering of the LUMO energy is likely owing to the enforcement of the approximate coplanarity and thus improved conjugation of the electron-deficient thiazole units with the indolo[3,2-*b*]carbazole backbone.

The spectra of $\mathbf{1}^{+}$-$\mathbf{4}^{+}$ were recorded in order to provide insight in to the nature of the electronic coupling in the monocations (Figure 8). $[(p\text{-}BrC_6H_4)_3N]SbCl_6$ proved competent as a one-electron oxidant of all four compounds **1**-**4**. According to Hush theory,[52,60] a NIR-range intervalence charge-transfer (IVCT) absorption is expected for the sufficiently delocalized mixed-valence state. Compound $\mathbf{1}^{+}$ showed no strong absorption in the NIR region, suggesting that the unpaired electron is largely localized in one of the pincer units and placing $\mathbf{1}^{+}$ into the Robin-Day class I. [51,52]

Compounds $\mathbf{2}^{+}$-$\mathbf{4}^{+}$ displayed multiple intensive but broad peaks in NIR region. The reason could be a vibronic progression, in which the absorption bands are coupled with C=C/C=N stretching modes, as was discussed for **G**, **H** (Figure 10) and related others.[61,62] The deconvolution of peaks (Figure 9) was conducted to obtain the accurate peak positions and the results were summarized in Table 5. In the purely organic analogue **G**[63] and the rhenium complex **F**[40] (Figure 10), which have been assigned as class III mixed-valence compounds, the Hush electron coupling integral $V = \nu_{max}/2$ are 3180 and 3715 cm^{-1}, respectively. In our case, V of $\mathbf{2}^{+}$ is 2876 cm^{-1}. Aside from the somewhat smaller V, $\mathbf{2}^{+}$ can be tentatively assigned as class III due to its electronic similarity and high K_c; however, the possibility of being class II cannot be totally ruled out. Compounds **3** and **4** are easier to assign since their V are 4736 and 3537 cm^{-1} (cf. 4765 cm^{-1} for **H**), values that are squarely in the range of class III. Notably, the trend **3** > **4** > **2** > **1** suggested by the NIR absorption spectroscopy is consistent with the K_c measurement in electrochemistry.

Addition of the second equivalent of the oxidant $[(p\text{-}BrC_6H_4)_3N]SbCl_6$ permitted in-situ observation of $\mathbf{1}^{++}$, $\mathbf{2}^{++}$, and $\mathbf{3}^{++}$. The major absorption feature of $\mathbf{1}^{++}$ was similar to $\mathbf{1}^{+}$, as should be expected if its charges are largely isolated. On the other hand, the intense absorptions in the NIR region of $\mathbf{2}^{+}$ and $\mathbf{3}^{+}$ disappeared and no new NIR features such as in $\mathbf{C}^{+}$ and the dications of ethynyl-bridged PNP dimers were evident.[19,32] The domination quinoidal structures of $\mathbf{2}^{++}$ and $\mathbf{3}^{++}$ (Figure 5) results in an electronic environment of ligand π* orbitals that is quite different from a radical species such as $\mathbf{C}^{+}$. On the other hand, the MLCT bands at around 600-700 nm increased in intensity upon second oxidation.

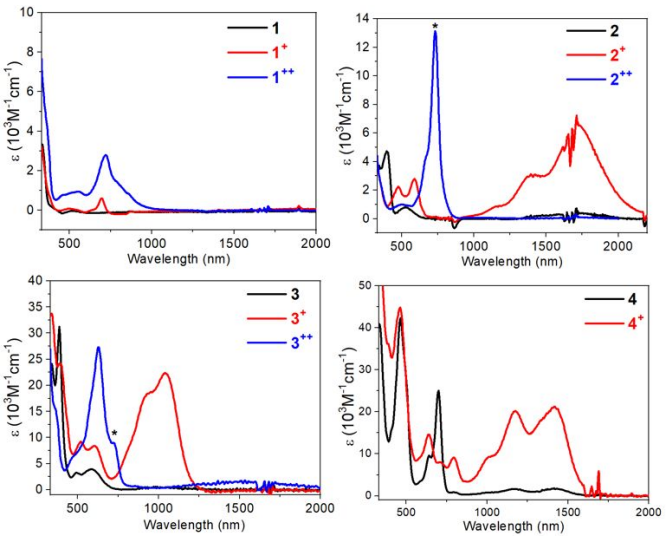

Figure 8. UV-Vis-NIR spectra of compounds **1**-**4** and their oxidized derivatives. The monocations were produced in situ via addition of 1 equiv. of oxidant ([Ox] = $(BrC_6H_4)_3N]SbCl_6$) solutions of **1**-**4** in CH_2Cl_2 and the dications were produced via addition of 2.2 equiv. of oxidant. The asterisk labels the possible overlapping at 732 nm of excess $(BrC_6H_4)_3N]SbCl_6$.

Treatment of **4** with $[(p\text{-}BrC_6H_4)_3N]SbCl_6$ did not lead to the clean formation of $\mathbf{4}^{++}$, consistent with the high 2nd oxidation potential determined for **4** in CV studies. Therefore, **4** was further studied using spectroelectrochemical measurements (Figure S54). A series of optical spectra was collected after

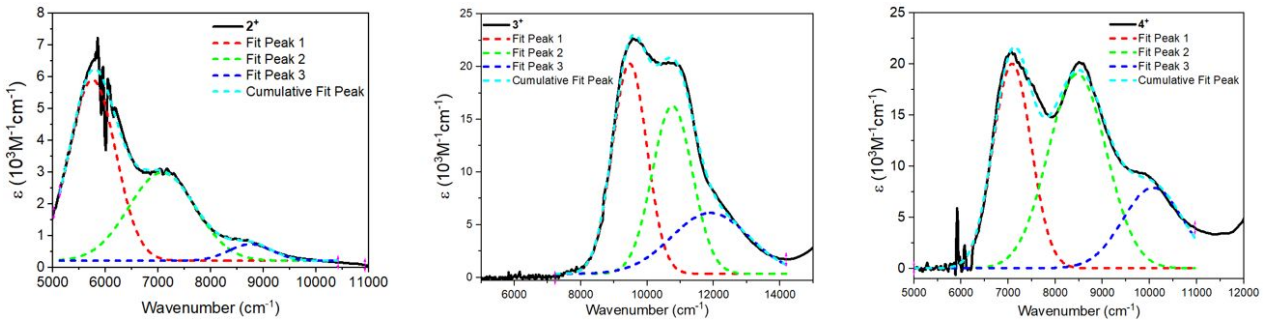

Figure 9. Deconvolution of low energy bands of $\mathbf{2}^{+}$-$\mathbf{4}^{+}$.

subjecting a solution of **4** containing $[^nBu_4N]PF_6$ as the electrolyte to different constant voltages for 5 min. This experiment allowed the observation of the spectrum of $\mathbf{4}^+$ (matching that obtained by chemical oxidation, Figure 8), and at higher potential, the spectrum of $\mathbf{4}^{++}$. The observed series of spectra displayed multiple isosbestic points, indicating quantitative oxidation processes and thus high stability of the oxidized cations.

Table 5. Spectral data of $\mathbf{2}^+$-$\mathbf{4}^+$ from Figure 9 (cm^{-1}).

Compound	Fit Peak 1	Fit Peak 2	Fit Peak 3
$\mathbf{2}^+$	5751	7069	8742
$\mathbf{3}^+$	9472	10759	11905
$\mathbf{4}^+$	7074	8476	10023

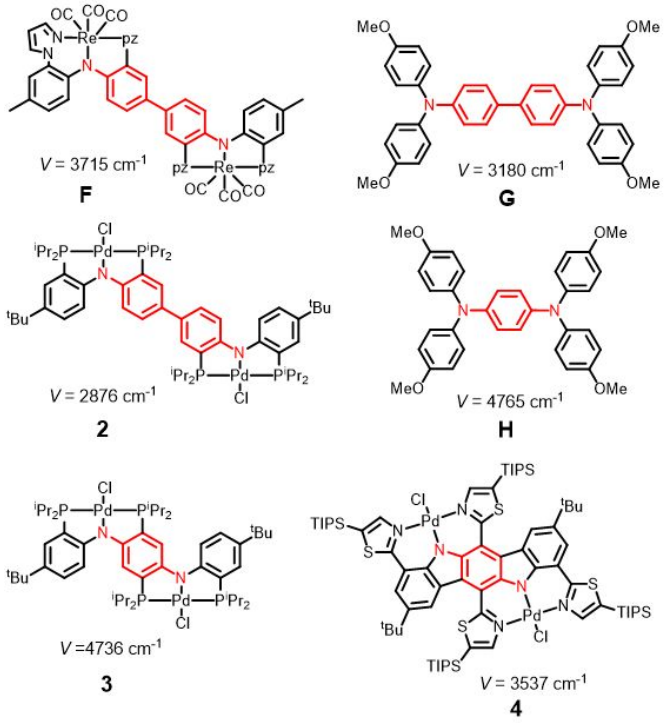

Figure 10. Hush coupling constants comparison.

Conclusions

In summary, we described how novel, highly conjugated and delocalized systems with two reversible redox events can be obtained from the linkage or fusion of two pincer complexes into a single molecule. Analysis of the bis(palladium) complexes by X-ray diffraction, cyclic voltammetry, UV-Vis-NIR and EPR spectroscopies, as well as DFT calculations suggests that in two or possibly three of the four systems, the mono-oxidized radical cation can be viewed as a highly delocalized mixed-valence state. The square-planar, divalent Pd center imposes a more rigid geometry on the organic ligand that leads to at least partial coplanarization of the aromatic rings of the extended system. The presence of the metal center is important in stabilizing the mono- and bis-oxidized forms of the molecule, even though the participation of metal d-orbitals in electronic delocalization is modest.

The greatest degree of electronic coupling was observed in the two fused bis(pincer) complexes built around a central *p*-diaminobenzene or an indolo[3,2-*b*]carbazole framework. The latter in particular contains an extended, flat and highly conjugated π-system that can be thought of as a fragment of a ladder metallapolymer. The bis(pincer) complexes studied in this work are potential building blocks for more complex conjugated molecules and potentially polymers. These compounds possess two Pd-Cl functionalities that should allow for straightforward synthetic modification in further studies.

Conflicts of interest

There are no conflicts to declare.

Acknowledgements

We are grateful to the Welch Foundation (grant A-1717 to O.V.O.) and the National Science Foundation (grant DMR-1654029 to L.F.) for support of this research. The authors thank Dr. Yi Liu, Teresa Chen and Liana Klivansky at Molecular Foundry, Lawrence Berkeley National Laboratory, for providing the instrument support for the spectroelectrochemistry measurements. Work at the Molecular Foundry was supported by the Office of Science, Office of Basic Energy Sciences, of the U.S. Department of Energy under Contract No. DE-AC02-05CH11231.

Notes and references

1 W.-H. Chen, K.-L. Wang, D.-J. Liaw, K.-R. Lee and J.-Y. Lai, N,N,N′,N′-Tetraphenyl-1,4-phenylenediamine−fluorene alternating conjugated polymer: synthesis, characterization, and electrochromic application, *Macromolecules*, 2010, **43**, 2236–2243.

2 H.-J. Yen and G.-S. Liou, Recent advances in triphenylamine-based electrochromic derivatives and polymers, *Polym. Chem.*, 2018, **9**, 3001–3018.

3 N. J. Jeon, J. Lee, J. H. Noh, M. K. Nazeeruddin, M. Grätzel and S. I. Seok, Efficient inorganic–organic hybrid perovskite solar cells based on pyrene arylamine derivatives as hole-transporting materials, *J. Am. Chem. Soc.*, 2013, **135**, 19087–19090.

4 M. Liang and J. Chen, Arylamine organic dyes for dye-sensitized solar cells, *Chem. Soc. Rev.*, 2013, **42**, 3453–3488.

5 Y. Tao, C. Yang and J. Qin, Organic host materials for phosphorescent organic light-emitting diodes, *Chem. Soc. Rev.*, 2011, **40**, 2943–2970.

6 M. Shimizu, R. Kaki, Y. Takeda, T. Hiyama, N. Nagai, H. Yamagishi and H. Furutani, 1,4-bis(diarylamino)-2,5-bis(4-cyanophenylethenyl)benzenes: fluorophores exhibiting efficient red and near-infrared emissions in solid state, *Angew. Chem. Int. Ed.*, 2012, **51**, 4095–4099.

7 M. Jonsson, D. Wayner and J. Lusztyk, *Redox and acidity properties of alkyl and arylamine radical cations and the corresponding aminyl radicals 1*, 1996, vol. 100.

8 J. Hioe, D. Šakić, V. Vrček and H. Zipse, The stability of nitrogen-centered radicals, *Org. Biomol. Chem.*, 2015, **13**, 157–169.

9 T. Büttner, J. Geier, G. Frison, J. Harmer, C. Calle, A. Schweiger, H.

Schönberg and H. Grützmacher, A stable aminyl radical metal complex, *Science*, 2005, **307**, 235.

10 S. Fortier, O. G. Moral, C.-H. Chen, M. Pink, J. J. Le Roy, M. Murugesu, D. J. Mindiola and K. G. Caulton, Probing the redox non-innocence of dinuclear, three-coordinate Co(II) nindigo complexes: not simply β-diketiminate variants, *Chem. Commun.*, 2012, **48**, 11082–11084.

11 M. T. Nguyen, R. A. Jones and B. J. Holliday, Understanding the effect of metal centers on charge transport and delocalization in conducting metallopolymers, *Macromolecules*, 2017, **50**, 872–883.

12 M. Gallei and C. Rüttiger, Recent trends in metallopolymer design: redox-controlled surfaces, porous membranes, and switchable optical materials using ferrocene-containing polymers, *Chem. – Eur. J.*, 2018, **24**, 10006–10021.

13 J.-C. Eloi, L. Chabanne, G. R. Whittell and I. Manners, Metallopolymers with emerging applications, *Mater. Today*, 2008, **11**, 28–36.

14 B. J. Holliday and T. M. Swager, Conducting metallopolymers: the roles of molecular architecture and redox matching, *Chem Commun*, 2005, 23–36.

15 A. I. Nguyen, R. A. Zarkesh, D. C. Lacy, M. K. Thorson and A. F. Heyduk, Catalytic nitrene transfer by a zirconium(IV) redox-active ligand complex, *Chem. Sci.*, 2011, **2**, 166–169.

16 A. F. Heyduk, R. A. Zarkesh and A. I. Nguyen, Designing catalysts for nitrene transfer using early transition metals and redox-active ligands, *Inorg. Chem.*, 2011, **50**, 9849–9863.

17 R. A. Zarkesh, J. W. Ziller and A. F. Heyduk, Four-electron oxidative formation of aryl diazenes using a tantalum redox-active ligand complex, *Angew. Chem. Int. Ed.*, 2008, **47**, 4715–4718.

18 A. T. Radosevich, J. G. Melnick, S. A. Stoian, D. Bacciu, C.-H. Chen, B. M. Foxman, O. V. Ozerov and D. G. Nocera, Ligand reactivity in diarylamido/bis(phosphine) PNP complexes of $Mn(CO)_3$ and $Re(CO)_3$, *Inorg. Chem.*, 2009, **48**, 9214–9221.

19 D. Adhikari, S. Mossin, F. Basuli, J. C. Huffman, R. K. Szilagyi, K. Meyer and D. J. Mindiola, Structural, spectroscopic, and theoretical elucidation of a redox-active pincer-type ancillary applied in catalysis, *J. Am. Chem. Soc.*, 2008, **130**, 3676–3682.

20 V. N. Madhira, P. Ren, O. Vechorkin, X. Hu and D. A. Vicic, Synthesis and electronic properties of a pentafluoroethyl-derivatized nickel pincer complex, *Dalton Trans.*, 2012, **41**, 7915–7919.

21 I. Kieltsch, G. G. Dubinina, C. Hamacher, A. Kaiser, J. Torres-Nieto, J. M. Hutchison, A. Klein, Y. Budnikova and D. A. Vicic, Magnitudes of Electron-withdrawing effects of the trifluoromethyl ligand in organometallic complexes of copper and nickel, *Organometallics*, 2010, **29**, 1451–1456.

22 J. J. Davidson, J. C. DeMott, C. Douvris, C. M. Fafard, N. Bhuvanesh, C.-H. Chen, D. E. Herbert, C.-I. Lee, B. J. McCulloch, B. M. Foxman and O. V. Ozerov, Comparison of the electronic properties of diarylamido-based PNZ pincer ligands: redox activity at the ligand and donor ability toward the metal, *Inorg. Chem.*, 2015, **54**, 2916–2935.

23 P. J. Chirik, Preface: Forum on redox-active ligands, *Inorg. Chem.*, 2011, **50**, 9737–9740.

24 V. Lyaskovskyy and B. de Bruin, Redox non-innocent ligands: versatile new tools to control catalytic reactions, *ACS Catal.*, 2012, **2**, 270–279.

25 B. de Bruin, P. Gualco and N. D. Paul, in *Ligand Design in Metal Chemistry*, John Wiley & Sons, Ltd, 2016, pp. 176–204.

26 P. J. Chirik and K. Wieghardt, Radical ligands confer nobility on base-metal catalysts, *Science*, 2010, **327**, 794.

27 C. Zhu, X. Ji, D. You, T. L. Chen, A. U. Mu, K. P. Barker, L. M. Klivansky, Y. Liu and L. Fang, Extraordinary redox activities in ladder-type conjugated molecules enabled by B ← N coordination-promoted delocalization and hyperconjugation, *J. Am. Chem. Soc.*, 2018, **140**, 18173–18182.

28 K. Arumugam, M. C. Shaw, P. Chandrasekaran, D. Villagrán, T. G. Gray, J. T. Mague and J. P. Donahue, Synthesis, structures, and properties of 1,2,4,5-benzenetetrathiolate linked group 10 metal Complexes, *Inorg. Chem.*, 2009, **48**, 10591–10607.

29 N. Deibel, M. G. Sommer, S. Hohloch, J. Schwann, D. Schweinfurth, F. Ehret and B. Sarkar, dinuclear quinonoid-bridged d^8 metal complexes with redox-active azobenzene stoppers: electrochemical properties and electrochromic behavior, *Organometallics*, 2014, **33**, 4756–4765.

30 A. M. Hollas, W. Gu, N. Bhuvanesh and O. V. Ozerov, Synthesis and characterization of Pd complexes of a carbazolyl/bis(Imine) NNN pincer ligand, *Inorg. Chem.*, 2011, **50**, 3673–3679.

31 D. E. Herbert and O. V. Ozerov, Binuclear palladium complexes supported by bridged pincer ligands, *Organometallics*, 2011, **30**, 6641–6654.

32 C.-H. Yu, X. Yang, X. Ji, C.-H. Wang, Q. Lai, N. Bhuvanesh and O. V. Ozerov, Redox communication between two diarylamido/bis(phosphine) (PNP)M moieties bridged by ynediyl linkers (M = Ni, Pd, Pt), *Inorg. Chem.*, 2020, **59**, 10153-10162.

33 Y. Li, Y. Wu and B. S. Ong, Polyindolo[3,2-b]carbazoles: A new class of p-channel semiconductor polymers for organic thin-film transistors, *Macromolecules*, 2006, **39**, 6521–6527.

34 P. Steenwinkel, H. Kooijman, W. J. J. Smeets, A. L. Spek, D. M. Grove and G. van Koten, Intramolecularly stabilized 1,4-phenylene-bridged homo- and heterodinuclear palladium and platinum organometallic complexes containing n,c,n-coordination motifs; η^1-SO_2 coordination and formation of an organometallic arenium ion complex with two Pt−C σ-bonds, *Organometallics*, 1998, **17**, 5411–5426.

35 S. L. Jeon, D. M. Loveless, W. C. Yount and S. L. Craig, Thermodynamics of pyridine coordination in 1,4-phenylene bridged bimetallic (Pd, Pt) complexes containing two N,C,N′ motifs, 1,4-M_2-$[C_6(CH_2NR_2)_4$-2,3,5,6], *Inorg. Chem.*, 2006, **45**, 11060–11068.

36 S. J. Loeb and G. K. H. Shimizu, Dimetallated thioether complexes as building blocks for organometallic coordination polymers and aggregates, *J. Chem. Soc. Chem. Commun.*, 1993, 1395–1397.

37 S. J. Loeb, G. K. H. Shimizu and J. A. Wisner, Mono- versus dipalladation of the durene-based tetrathioether ligand 1,2,4,5-$(tBu_5CH_2)_4C_6H_2$. Structures of $[PdCl((^tBuSCH_2)_4C_6H)]$ and $[Pd_2((^tBuSCH_2)_4C_6)(MeCN)_2][BF_4]_2$, *Organometallics*, 1998, **17**, 2324–2327.

38 D. Das, P. Singh, M. Singh and A. K. Singh, Tetradentate selenium ligand as a building block for homodinuclear complexes of Pd(II) and Ru(II) having seven membered rings or bis-pincer coordination mode: high catalytic activity of Pd-complexes for Heck reaction, *Dalton Trans.*, 2010, **39**, 10876–10882.

39 N. P. N. Wellala, H. T. Dong, J. A. Krause and H. Guan, Janus POCOP Pincer Complexes of Nickel, *Organometallics*, 2018, **37**, 4031–4039.

40 J. R. Gardinier, J. S. Hewage, B. Bennett, D. Wang and S. V. Lindeman, Tricarbonylrhenium(I) complexes of dinucleating redox-active pincer ligands, *Organometallics*, 2018, **37**, 989–1000.

41 L. Fan, L. Yang, C. Guo, B. M. Foxman and O. V. Ozerov, N−C cleavage in pincer PNP complexes of palladium, *Organometallics*, 2004, **23**, 4778–4787.
42 O. V. Ozerov, in *The Chemistry of Pincer Compounds*, eds. D. Morales-Morales and C. M. Jensen, Elsevier Science B.V., Amsterdam, 2007, pp. 287–309.
43 B. H. Yang and S. L. Buchwald, Palladium-catalyzed amination of aryl halides and sulfonates, *J. Organomet. Chem.*, 1999, **576**, 125–146.
44 J. F. Hartwig, Carbon−heteroatom bond-forming reductive eliminations of amines, ethers, and sulfides, *Acc. Chem. Res.*, 1998, **31**, 852–860.
45 J. F. Hartwig, Transition metal catalyzed synthesis of arylamines and aryl ethers from aryl halides and triflates: scope and mechanism, *Angew. Chem. Int. Ed.*, 1998, **37**, 2046–2067.
46 C. Cordovilla, C. Bartolomé, J. M. Martínez-Ilarduya and P. Espinet, The Stille reaction, 38 years later, *ACS Catal.*, 2015, **5**, 3040–3053.
47 J. Hämmerle, M. Schnürch, N. Iqbal, M. D. Mihovilovic and P. Stanetty, A guideline for the arylation of positions 4 and 5 of thiazole via Pd-catalyzed cross-coupling reactions, *Tetrahedron*, 2010, **66**, 8051–8059.
48 R. F. Winter, Half-wave potential splittings $\Delta E_{1/2}$ as a measure of electronic coupling in mixed-valent systems: triumphs and defeats, *Organometallics*, 2014, **33**, 4517–4536.
49 R. J. Crutchley, in *Advances in inorganic chemistry*, ed. A. G. Sykes, Academic Press, 1994, vol. 41, pp. 273–325.
50 D. M. D'Alessandro and F. R. Keene, A cautionary warning on the use of electrochemical measurements to calculate comproportionation constants for mixed-valence compounds, *Dalton Trans.*, 2004, 3950–3954.
51 M. B. Robin and P. Day, in *Advances in inorganic chemistry and radiochemistry*, eds. H. J. Emeléus and A. G. Sharpe, Academic Press, 1968, vol. 10, pp. 247–422.
52 K. D. Demadis, C. M. Hartshorn and T. J. Meyer, The localized-to-delocalized transition in mixed-valence chemistry, *Chem. Rev.*, 2001, **101**, 2655–2686.
53 W. Lamm, F. Pragst and W. Jugelt, Untersuchungen zum anodischen verhalten von carbazolen und indolo[3,2-b]carbazolen in acetonitril, *J. Für Prakt. Chem.*, 1975, **317**, 995–1004.
54 L. Fan, B. M. Foxman and O. V. Ozerov, N−H cleavage as a route to palladium complexes of a new pnp pincer ligand, *Organometallics*, 2004, **23**, 326–328.
55 S. Stoll and A. Schweiger, EasySpin—A comprehensive software package for spectral simulation and analysis in EPR, *J. Magn. Reson. San Diego Calif 1997*, 2006, **178**, 42–55.
56 P. J. Hay and W. R. Wadt, Ab initio effective core potentials for molecular calculations. Potentials for K to Au including the outermost core orbitals, *J. Chem. Phys.*, 1985, **82**, 299–310.
57 X.-S. Ke, Y. Hong, P. Tu, Q. He, V. M. Lynch, D. Kim and J. L. Sessler, Hetero Cu(III)–Pd(II) complex of a dibenzo[g,p]chrysene-fused bis-dicarbacorrole with stable organic radical character, *J. Am. Chem. Soc.*, 2017, **139**, 15232–15238.
58 J. C. DeMott, N. Bhuvanesh and O. V. Ozerov, Frustrated Lewis pair-like splitting of aromatic C–H bonds and abstraction of halogen atoms by a cationic [(FPNP)Pt]+ species, *Chem. Sci.*, 2013, **4**, 642–649.
59 Ultraviolet, visible, and near-infrared spectra.60 N. S. Hush, Distance dependence of electron transfer rates, *Coord. Chem. Rev.*, 1985, **64**, 135–157.
61 C. Risko, V. Coropceanu, S. Barlow, V. Geskin, K. Schmidt, N. E. Gruhn, S. R. Marder and J.-L. Brédas, Trends in electron-vibration and electronic interactions in bis(dimethylamino) mixed-valence systems: a joint experimental and theoretical investigation, *J. Phys. Chem. C*, 2008, **112**, 7959–7967.
62 V. Coropceanu, M. Malagoli, J. M. André and J. L. Brédas, Charge-transfer transitions in triarylamine mixed-valence systems: a joint density functional theory and vibronic coupling study, *J. Am. Chem. Soc.*, 2002, **124**, 10519–10530.
63 C. Lambert and G. Nöll, The class II/III transition in triarylamine redox systems, *J. Am. Chem. Soc.*, 1999, **121**, 8434–8442.